International Journal of Automotive Technology, Vol. 14, No. 5, pp. 731–737 (2013)
DOI 10.1007/s12239–013–0080–5

pISSN 1229–9138/ eISSN 1976–3832

DESIGN OF VEHICLE OF ON-GLASS 4×4 MIMO ANTENNAS FOR WIBRO APPLICATIONS

S. B. AHN[1] and H. S. CHOO[2]*

[1]RFID/USN) Consulting & Development Team, LS Industrial Systems Co., Ltd., Anyang-si, Gyeonggi 431-749, Korea
[2]School of Electronic and Electrical Engineering, Hongik University, Seoul 121-791, Korea

(Received 22 November 2012; Revised 30 January 2013; Accepted 25 February 2013)

ABSTRACT–This paper proposes on-glass 4×4 MIMO antennas with broad bandwidth and high radiation gain, suitable for receiving WiBro internet applications in a commercial sedan. For the individual antenna body, we used a triangular-shaped patch that most efficiently satisfies broad-matching bandwidth. Then the inside of the triangular patch was partially removed to broaden the driver's field of view. To obtain detailed design parameters that exhibit optimum radiating performance, we used a genetic algorithm (GA) in conjunction with a full wave EM simulator and varied the feeding locations of four antennas so as to increase throughput capacity for effective data transmission. The proposed antenna showed -10 dB matching bandwidth and a measured average gain of about 4.77 dBi along the bore-sight direction ($\theta = 90°$, $\phi = 180°$) in the entire WiBro band (2.3-2.4 GHz). To confirm the MIMO performance in a real situation, we measured the commercial WiBro signal using the proposed antennas in an urban environment. The correlation coefficients among the antennas were calculated, and the result revealed an average value of 0.105.

KEY WORDS : On-glass antenna, Vehicle antennas, MIMO antennas, WiBro antennas

1. INTRODUCTION

Recently, mobile internet services such as the wireless fidelity (Wi-Fi), high-speed downlink packet access (HSDPA), and wireless broadband (WiBro) have been launched in Korea (Lee *et al.*, 2007). With the advance of mobile internet services, the vehicle industry has a new-found interest in integrating internet service transceivers into their products. In particular, WiBro, considered most appropriate for commercial vehicles, can handle high data rates and has good mobility characteristics. For example, WiBro can have an uplink of 5.2 Mbps and a downlink of 24.8 Mbps at vehicles' speeds of up to 120 km/h (Yang *et al.*, 2007). Generally, portable WiBro transceivers use a single pole-type antenna integrated into the system. However, such integrated antennas may have drastically reduced antenna gain by a body blockage effect and result in low throughput capacity. This occurs because in a vehicle, the antenna and its related systems are usually placed deep inside the vehicle near the front control unit. In addition, the single integrated antenna may show even more decreased throughput capacity when the vehicle moves through the urban environment where multi-path fading dominates the channel characteristics (Vaughan and Anderson, 1987; Foschini and Gans, 1998). To mitigate these problems, antennas that can minimize the body blockage effect are highly desirable. Accordingly, the situation calls for a communication method such as multi-input multi-output (MIMO) that can increase the throughput capacity of the data using multiple antennas (Gesbert *et al.*, 2002; Winters *et al.*, 1994).

In this paper, we propose on-glass WiBro MIMO antennas that consist of four individual antennas installed directly onto a vehicle's rear window. We employed a planar triangular patch as the basic antenna structure to increase the low input resistance of the on-glass antennas. Then, we partly removed the inside of the triangular patch to form a more visually transparent shape as well as to reduce the body blockage effect. To obtain more detailed design parameters exhibiting optimum radiating performance, we used a genetic algorithm (GA) in conjunction with a full wave electromagnetic (EM) simulator (Horn *et al.*, 1994; Hiroyasu *et al.*, 2000; Rahmat-Samii and Michielssen, 1999). In our EM simulation, we modeled the entire vehicle as piece-wise triangular and wire meshes according to the current distribution to obtain an accurate solution with a reduced simulation time. The designed antennas were mounted onto the rear window of a commercial sedan, and the antenna characteristics, such as the matching bandwidth and radiation pattern, were measured in an open site. Then, to maximize the channel capacity, the optimum feeding locations were examined by varying the distances among the individual antennas. Correlation coefficients

*Corresponding author. e-mail: hschoo@hongik.ac.kr

among the four antennas were calculated from 3D-radiation patterns, and an Ergodic channel capacity of the Rayleigh channel (representing the multi-path fading in urban environments) was obtained using the correlation coefficients (Dong *et al.*, 2005). To confirm the channel capacity performance, we also measured the received power of the proposed antennas in the WiBro service zone, which revealed low correlation coefficients of 0.105 among the received signals from the individual antennas.

This paper is organized as follows. Section II presents the geometry and measurement results of the proposed individual WiBro antenna. Section III describes the optimum feeding locations of each antenna and MIMO performance through a field test in an urban environment, and Section IV presents our conclusions.

2. DESIGN OF AN INDIVIDUAL ON-GLASS ANTENNA

2.1. Individual Antenna Structure and Optimization

The on-glass antennas appear to have strong potential for the vehicle WiBro application using the frequency range of 2.3-2.4 GHz; they have less performance deg-radation from the body blockage effect and better appearance compared to a pole-type antenna installed near a vehicle's front control units. However, the on-glass antenna working at such a high frequency range usually shows very low input resistance since the body of the antenna is placed in close proximity to the conducting frame of a vehicle. To resolve this problem, we employed a planar triangular-patch structure as the antenna body as shown in Figure 1. The antenna was fed by a 50 Ω coaxial cable from the left side of the rear window. The outer conductor of a coaxial cable was connected to the ground and the inner conductor was connected to the stripline of the antenna body. A thin Teflon layer inserted between the ends of the cable ensured a good connection. To obtain an input resistance close to 50 Ω, we adjusted the flare angle of the patch since the input resistance of the triangular shaped patch can be varied depending on the flare angle (Lin and Tasi, 1998). Also, the inside of the triangular patch was partly removed so as not to obstruct the driver's field of view to estimate the antenna performance, such as reflection coefficient and radiation gain, we used FEKO of *EM Software and Systems*. For accurate performance estimation, we considered the whole vehicle body in the EM simulation. However, the full mesh model took more than 12 hours with our computational resource (a quad CPU with 2.40 GHz and a memory size with 16 GHz). Therefore, to reduce the computational time to less than 20 minutes, we employed a hybrid mesh method using both triangular and wire meshes based on the amplitude of current distributions. We reduced the number of meshes by placing the triangular meshes where strong currents flowed. The remaining parts were modeled using

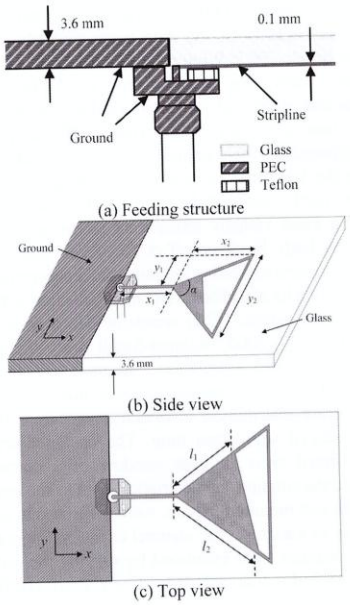

Figure 1. Triangular-shaped patch structure.

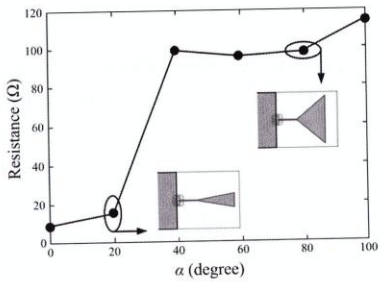

Figure 2. Input resistance depending on the flare angle α.

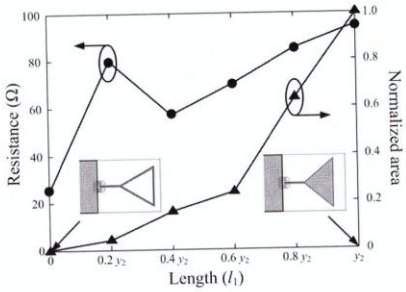

Figure 3. Input resistance depending on the surface area.

the wire meshes where weak currents flowed. The simulated radiation pattern using our hybrid mesh method had very similar radiation pattern to the measurement. Figure 2 exhibits a variation of input resistance depending on the flare angle α of the triangular patch. As the angle α increases, the input resistance of the antenna also increases. Thus, to match with 50 Ω coaxial cable, the flare angle α should be greater than 40°. We also examined the variation of the input resistance according to the filled area of the triangular patch as shown in Figure 3. The side length of the outer equilateral triangle patch and the flare angle α were fixed (y_2 = 41 mm, α = 60°) and then the length of the inner patch l_1 was gradually increased. In the figure, the normalized area was defined by the ratio of the inner filled area to the total triangular patch. The input resistance of the antenna increased when l_1 was enlarged. Considering the input resistance and driver's field of view, appropriate lengths of the inner patch can be determined approximately between 0.2 y_2 and 0.6 y_2. We also examined the variation of the azimuth gain according to the lengths of inner patch l_1 and l_2 as shown in Table 1.

The average gain of the antenna along the azimuth direction increased when l_2 was enlarged compared to l_1. To obtain more improved antenna performance, such as a broad matching bandwidth and a high radiation gain, the design parameters were more optimized using a Pareto genetic algorithm (PGA). In our PGA optimization process, the fitness functions were defined as follows:

$$\begin{aligned} fitness1 &= 1\text{-}S_{11}(f_j) \\ fitness2 &= \frac{1}{N \cdot M}\sum_{i=1}^{N}\sum_{j=1}^{M}\{\mathrm{Gain}(\phi_i, f_j)\} \\ &\quad where\left(\begin{matrix}\phi_i = 0 \sim 360^\circ, \theta = 90^\circ \\ 2.30\ \mathrm{GHz} \le f_j \le 2.40\ \mathrm{GHz}\end{matrix}\right) \\ filling\ area &= \left\{\frac{l_1 \times l_2}{\sqrt{x_2^2+y_1^2} \times \sqrt{x_2^2+(y_2-y_1)^2}}\right\} \times 100 \end{aligned} \quad (1)$$

The fitness 1 and fitness 2 functions represent the impedance matching and the average gain along the azimuth plane in the WiBro frequency band (2.3-2.4 GHz). Here f_j means the frequency points (f_j are 2.30, 2.32, 2.34, … , 2.40 GHz) of entire WiBro band, ϕ_i represents azimuth angle (ϕ_i are 0, 60, 120, …, 300°) of incident field. In our GA process, we filtered out the samples with a filling area of greater than 50% to adjust the driver's field of view.

Table 1. Performance comparisons by the changing lengths of the inner triangular patch.

l_1 / l_2	8 mm	16 mm	24 mm	32 mm
8 mm	-3.514 dBi	-2.800 dBi	-3.295 dBi	-3.202 dBi
16 mm	-2.152 dBi	-3.155 dBi	-3.453 dBi	-5.823 dBi
24 mm	-3.247 dBi	-3.417 dBi	-3.820 dBi	-3.128 dBi
32 mm	-2.957 dBi	-3.371 dBi	-3.070 dBi	-3.119 dBi

Table 2. Dimensions of the optimized antenna.

Parameter	x_1	x_2	y_1	y_2	a	l_1	l_2
Value (mm)	16.9	35.5	20.5	41	60°	10	14

2.2. Measurement Results for the Individual Antenna

Table 2 lists the optimized design parameters. The optimized antenna was printed on a rear window of a commercial sedan (2007 Hyundai Grandeur TG Q 240). To measure the individual antenna's performance, we used the broadband horn antenna (Schwarzbeck Mess BBHA 9120D) with an Agilent 8753D network analyzer. S-parameter was measured in an open site instead of measuring the antenna gain in anechoic chamber. Figure 4 shows the measured (solid line) and simulated (dashed line) reflection coefficient of the optimized antenna. The measured result is similar to the simulation, and it shows a bandwidth of around 20% (reflection coefficient < -10 dB for 2.2 GHz – 2.6 GHz) (Balanis, 2005). Figure 5 represents the measured and simulated bore-sight gain (ϕ = 180°, θ = 90°). The proposed antenna shows the bore-sight gain of more than 0 dBi in the WiBro frequency band and 4.77 dBi averaged

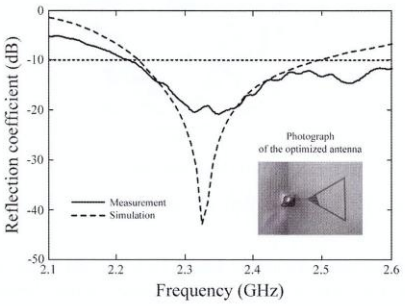

Figure 4. Reflection coefficient of the antenna.

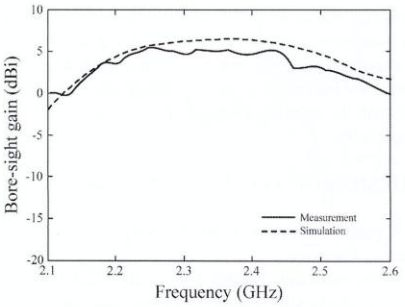

Figure 5. Bore-sight gain of the antenna.

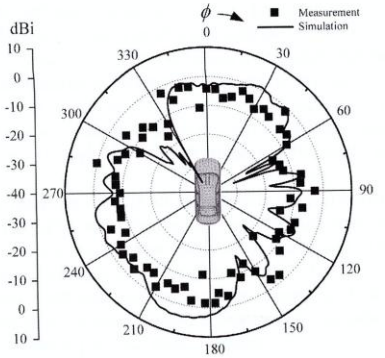

(a) Vertical gain

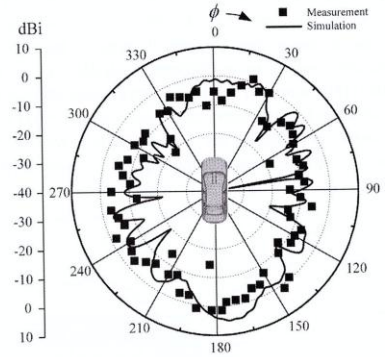

(b) Horizontal gain

Figure 6. Radiation pattern of the antenna.

over the same frequency band. This is 2 dB higher gain than that was obtained with a conventional monopole printed on the same window. We also measured the radiation pattern of the proposed antenna in azimuth direction ($\theta = 90°$). Figure 6 (a) and (b) ilustrate the vertical and horizontal gains of the radiation patterns, respectively. The measured radiation patterns (solid line) agree well with the simulated radiation patterns (dashed line). The measured vertical and horizontal gains of -7.11 dBi and -6.85 dBi agree well with the simulated values of -6.49 dBi and -6.88 dBi, respectively.

3. DESIGN OF 4×4 MIMO ANTENNAS

3.1. Optimization of 4×4 MIMO Antennas for Maximum Channel Capacity

Channels exhibiting strong multi-path fading characteristics can drastically reduce the throughput capacity of the wireless internet in vehicles when the vehicles move through urban environments. Applying the MIMO antenna technology to a vehicle's built-in wireless internet system can improve the throughput capacity in such circumstances. The throughput capacity of the MIMO system is determined by correlation coefficients that are varying according to the position, distance, and polarization of the individual antennas. Therefore we examined the optimum positions of the four individual antennas on the rear window to realize a 4×4 MIMO antenna system with a maximum channel capacity. To estimate the channel capacity accurately, we first calculated the correlation coefficients among antennas as follows:

$$\psi_{ij} = \frac{1}{\sigma_i \sigma_j} \oint E\{(A_i(\Omega) \cdot E(\Omega))(A_j^*(\Omega) \cdot E^*(\Omega))\} d\Omega \quad (2)$$

where $A_i(\Omega)$ and $A_j(\Omega)$ are simulated 3D-radiation patterns of the individual antennas i and j, and $E(\Omega)$ is a random incident field (Dong *et al.*, 2005). The elevation angle of the incident field has Gaussian distribution with a mean of $\theta = 90°$ and a variance of 30°, while the azimuth angle of the incident field has a uniform distribution. σ represents the variance of the multiplication between the $A(\Omega)$ and $E(\Omega)$. Based on the correlation coefficients among the four antennas, we calculated the Ergodic channel capacity (Glodsmith and Varaiya, 1997).

$$C = E\left\{ log_2\left[det\left(I_{n_R} + \frac{\rho}{n_T} \tilde{H} \Psi \tilde{H}^* \right) \right] \right\} \quad (3)$$

where n_T and n_R are the numbers of transmitting and

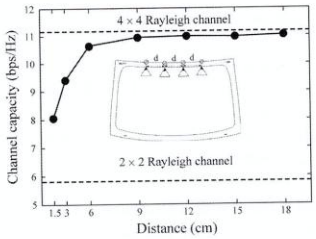

(a) Channel capacity when feeders are placed at upper frame

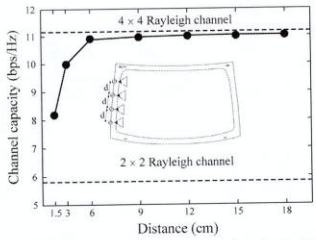

(b) Channel capacity when feeders are placed at side frame

Figure 7. Channel capacity according to the feeders locations.

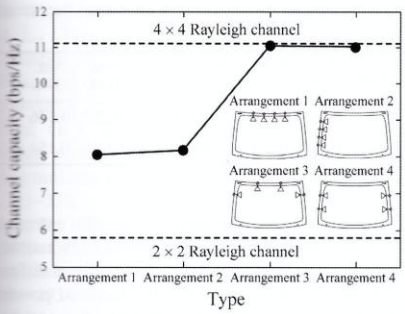

Figure 8. Channel capacity according to the antenna arrangements.

receiving antennas, $\tilde{H}$ is an $n_T \times n_R$ normalized transfer matrix in a flat-fading channel, and r is a signal to noise ratio. Figure 7 shows the channel capacity results with all four antennas placed at the upper and side frame of the rear window. We examined the channel capacity by varying the distance d among the antennas. For example, the channel capacity was 8 bps/Hz when d was around 3 cm, it increased up to 11 bps/Hz when d increased to 9 cm as shown in Figure 7 (a). Similarly, the channel capacity of 8 bps/Hz was obtained with d at 3 cm, when all four antennas were placed at the side frame.

To search the optimal placements for the antennas, we tried all four possible combinations as shown in Figure 8, and found that arrangement 3 exhibited the highest channel capacity of about 11.03 bps/Hz. This occurs due to the fact that arrangement 3 can offer the highest space diversity as well as the polarization diversity. To observe the MIMO performance more closely, we compared the channel capacity of the proposed antennas to the pole-type antennas' channel capacity as shown in Figure 9. We replaced the proposed antenna by the pole-type antenna and kept antenna positions the same. The results of the optimized antenna

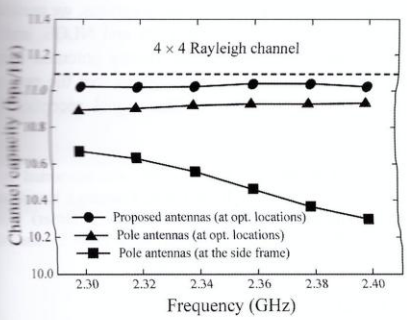

Figure 9. Comparisons of the channel capacity between the proposed antenna and the pole-type antenna.

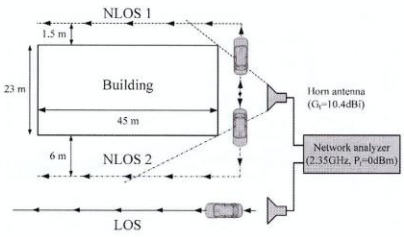

Figure 10. Measurement setup for the field test.

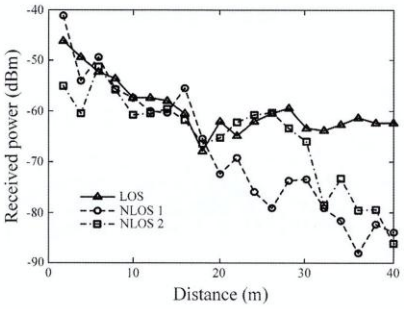

Figure 11. Received power by Ant. 1.

show 0.2 higher channel capacity compared to a conventional pole-type antenna.

3.2. Field Test Results of 4×4 MIMO Antennas

To confirm MIMO performance, we measured the received WiBro signal strength in two different situations. In the first measurement setup, we used the transmitting antenna of a Schwarzbeck Mess BBHA 9120D (Gain = 10.4 dBi) with an input power of 0 dBm. We then measured the received powers using our proposed antennas with an Agilent 8593A spectrum analyzer. The measurement sites

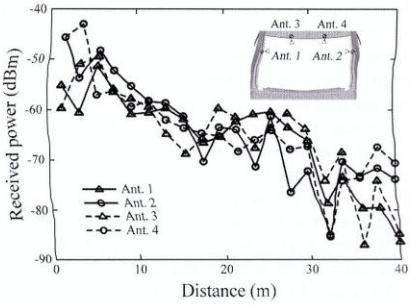

Figure 12. Received power by the four antennas from NLOS 2.

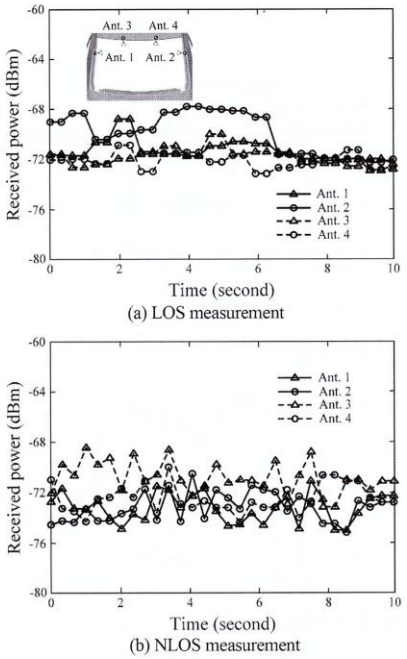

(a) LOS measurement

(b) NLOS measurement

Figure 13. Received signal power by the four antennas when driving the vehicle.

were classified by two cases based on line-of-site (LOS) and non-line-of-site (NLOS). The NLOS was also classified by NLOS1 (1.5 m) and NLOS2 (6 m) based on the distance from the building as shown in Figure 10. Figure 11 illustrates the received power by Ant. 1, with the results gathered from LOS (solid line), NLOS 1 (dashed line), and NLOS 2 (dash-dotted line). The received power of LOS declined proportionally with the square of the distance, but in the case of NLOS 1 and NLOS 2 it declined by more than the square of the distance as expected. The difference of the received power between LOS and NLOS was more than 20 dB when the distance was about 40 m. Figure 12 shows the received power of the four antennas in NLOS 2. As a result, the received powers exhibited oscillatory instability at each point and drastically decreased with the distance more than 30 m.

We intended the second set up to test the MIMO performance for a real time commercial WiBro signal (KT Show WiBro: 2.3315 GHz - 2.3585 GHz) using the proposed antennas from actual outdoor circumstances. The vehicle moved at a speed of 20 km/h, and the travel distance was 300 m. Data was collected using a laptop computer connected to a spectrum analyzer by a USB-GPIB controller. Figure 13 exhibits the received signal power by the four antennas for 10 seconds. The received power levels of LOS maintained a relatively stable level in all cases with the level difference about 4 dB. On the other hand, the received powers of NLOS were very different; they varied rapidly according to the time of measurement. Then the correlation coefficients among the received signals of the four antennas were calculated as shown in Table 3. In LOS, the correlation coefficients averaged over 10 seconds duration were ranged from 0.15 to 0.32, and the average for six cases was 0.218. In NLOS, the correlation coefficients ranged from 0.05 to 0.17, and the average for six cases was very low at about 0.105.

Table 3. Correlation coefficients among the received powers.

Correlation	Ant. 1–2	Ant. 1–3	Ant. 1–4	Ant. 2–3	Ant. 2–4	Ant. 3–4	Total
LOS	0.322	0.177	0.206	0.205	0.252	0.146	0.218
NLOS	0.074	0.108	0.064	0.175	0.055	0.154	0.105

4. CONCLUSION

In this paper, we proposed 4×4 on-glass MIMO antennas with broad bandwidth and high radiation gain for WiBro applications in vehicles. We optimized a planar triangular patch structure to increase the low input resistance of the on-glass antenna. To improve the driver's field of view, the inside of the triangular patch was partially removed. The proposed antenna was built and mounted on the rear window of a sedan, and then antenna characteristics such as reflection coefficient and radiation pattern were measured. The measurement showed a -10 dB matching bandwidth and average gain of about 5 dBi along the bore-sight direction in the entire WiBro band. The feeding locations of the four antennas were also optimized to maximize the channel capacity by varying the distance among the individual antennas. Using our proposed antennas with the optimum feeding locations, we measured the real time WiBro signals in LOS and NLOS, and the resulting correlation coefficients among antennas ranged from 0.105 to 0.218. Our results reveal that the proposed antenna is well-suited for WiBro signal reception in a vehicle.

ACKNOWLEDGMENT–This research was supported by the MSIP (Ministry of Science, ICT&Future Planning), Korea, under the ITRC (Information Technology Research Center) support program (NIPA-2013-H0301-13-2007) supervised by the NIPA (National IT Industry Promotion Agency).

REFERENCES

Balanis, C. A. (2005). *Antenna Theory and Design*, 3rd

edn. Wiley. New York.
Dong, L., Choo, H., Heath, R. W. and Ling, H. (2005). Simulation of MIMO channel capacity with antenna polarization diversity. *IEEE Trans. Wireless Comm.* **4**, **4**, 1869–1873.
Foschini, G. J. and Gans, M. J. (1998). On limits of wireless communications in a fading environment when using multiple antennas. *Wireless Personal Commun.* **6**, 3, 311–335.
Gesbert, D., Bölcskei, H., Gore, D. A. and Paulraj, A. J. (2002). Outdoor MIMO wireless channels: Models and performance prediction. *IEEE Trans. Commun.* **50**, **12**, 1926–1934.
Goldsmith, A. and Varaiya, P. (1997). Capacity of fading channels with channel side information. *IEEE Trans. Inform. Theory* **43**, **6**, 1986–1992.
Hiroyasu, T., Miki, M. and Watanabe, S. (2000). The new model of parallel genetic algorithm in multi-objective optimization problems-divided range multi-objective genetic algorithm. *Proc. Evolutionary Computation Conf.*, **1**, 333–340.
Horn, J., Nafpliotis, N. and Goldberg, D. E. (1994). A niched Pareto genetic algorithm for multiobjective optimization. *Proc. Evolutionary Computation Conf.*, **1**, 82–87.
Lee, W., Kang, S., Lim, S., Shin, M. and Kim, Y. (2007). Adaptive hierarchical surrogate for searching web with mobile devices. *IEEE Trans. Consumer Electronics* **53**, **2**, 769–803.
Lin, Y. and Tasi, S. (1998). Analysis and design of broadside-coupled striplines-fed bow-tie antennas. *IEEE Trans. Antennas Propag.* **46**, **3**, 459–460.
Rahmat-Samii, Y. and Michielssen, E. (1999). *Electromagnetic Optimization by Genetic Algorithms*. Wiley. New York.
Vaughan, R. G. and Andersen, J. B. (1987). Antenna diversity in mobile communications. *IEEE Trans. Vehicle Technology* **36**, **4**, 149–172.
Winters, J. H., Salz, J. and Gitlin, R. D. (1994). The impact of antenna diversity on the capacity of wireless communications systems. *IEEE Trans. Commun.* **42**, **2**, 1740–1751.
Yang, K., Ou, S., Chen, H. and He, J. (2007). Multihop peer-communication protocol with fairness guarantee for IEEE 802.16-based vehicular networks. *IEEE Trans. Vehicle Technology* **56**, **6**, 3358–3370.